IVYSPRING INTERNATIONAL PUBLISHER

Theranostics

2017; 7(1): 51-66. doi: 10.7150/thno.16074

Research Paper

Localized Delivery of shRNA against PHD2 Protects the Heart from Acute Myocardial Infarction through Ultrasound-Targeted Cationic Microbubble Destruction

Li Zhang[1*], Zhenxing Sun[1*], Pingping Ren[1], Manjie You[1], Jing Zhang[1], Lingyun Fang[1], Jing Wang[1], Yihan Chen[1], Fei Yan[2]✉, Hairong Zheng[2]✉, Mingxing Xie[1]✉

1. Department of Ultrasound, Union Hospital, Tongji Medical College, Huazhong University of Science and Technology, Hubei Province Key Laboratory of Molecular Imaging, Wuhan, China;
2. Paul C. Lauterbur Research Center for Biomedical Imaging, Institute of biomedical and Health Engineering, Shenzhen Institutes of Advanced Technology, Chinese Academy of Sciences, Shenzhen, China.

*Both authors contributed equally to this manuscript.

✉ Corresponding authors: Mingxing Xie, MD. 1277 Jeifang Avenue, Wuhan 430022, China. E-mail: xiemx64@126.com; Telephone: +86 27 85726386. Or Fei Yan and Hairong Zheng, PhD. 1068 Xueyuan Avenue, Shenzhen University Town, Shenzhen 518055, China. E-mails: fei.yan@siat.ac.cn and hr.zheng@siat.ac.cn; Telephone: +86 755 86392284, Fax: +86 755 96382299.

Received: 2016.05.06; Accepted: 2016.08.30; Published: 2017.01.01

Abstract

Hypoxia-inducible factor 1α (HIF-1α) plays a critical protective role in ischemic heart disease. Under normoxic conditions, HIF-1α was degraded by oxygen-dependent prolyl hydroxylase-2 (PHD2). Gene therapy has become a promising strategy to inhibit the degradation of HIF-1α and to improve cardiac function after ischemic injury. However, conventional gene delivery systems are difficult to achieve a targeted and localized gene delivery into the ischemic myocardia. Here, we report the localized myocardial delivery of shRNA against PHD2 through ultrasound-targeted microbubble destruction (UTMD) for protection the heart from acute myocardial infarction. In this study, a novel cationic microbubble was fabricated by using of the thin-film hydration and sonication method. The resulting microbubbles had a 28.2 ± 2.21 mV surface zeta potential and could greatly improve DNA binding performance, achieving 17.81 ± 1.46 μg of DNA loading capacity per 5 × 10^8 microbubbles. Combined with these cationic microbubbles, UTMD-mediated gene delivery was evaluated and the gene transfection efficiency was optimized in the H9C2 cardiac cells. Knockdown of PHD2 gene was successfully realized by UTMD-mediated shPHD2 transfection, resulting in HIF-1α-dependent protective effects on H9C2 cells through increasing the expression of HIF-1α, VEGF and bFGF. We further employed UTMD-mediated shPHD2 transfection into the localized ischemic myocardia in a rat ischemia model, demonstrating significantly reduced infarct size and greatly improved the heart function. The silencing of PHD2 and the up-regulation of its downstream genes in the treated myocardia were confirmed. Histological analysis further revealed numbers of HIF-1α- and VEGF-, and CD31-positive cells/mm^2 in the shPHD2-treated group were significantly greater than those in the sham or control vector groups ($P < 0.05$). In conclusion, our study provides a promising strategy to realize ultrasound-mediated localized myocardial shRNA delivery to protect the heart from acute myocardial infarction via cationic microbubbles.

Key words: Prolyl hydroxylase-2, Ischemic myocardial disease, Gene delivery, Ultrasound, Cationic microbubbles.

Introduction

Ischemic heart disease remains the major cause of mortality worldwide despite advancements in clinical management [1]. Pathologically, there is an imbalance between myocardial oxygen supply and demand following an ischemic injury, resulting in myocardial hypoxia and the accumulation of waste

metabolites [2]. During acute hypoxia or ischemia, hypoxia-inducible factor 1α (HIF-1α), which plays a critical protective role in ischemic heart disease, is up-regulated. Physiologically, HIF-1α has been known as the most pivotal regulator to maintain oxygen homeostasis by getting involved in various biological processes such as angiogenesis, vascular remodeling, glucose metabolism and redox homeostasis [3]. However, HIF-1α is easily degraded by oxygen-dependent prolyl hydroxylase-2 (PHD2) under normoxic conditions [4]. Therefore, inhibition of HIF-1α degradation has become a promising strategy to improve cardiac function after ischemic injury [5].

Cardiac gene therapy has been applied in experimental and clinical studies. Different gene delivery systems for cardiac gene therapy have recently been developed [6]. Most of them lack targeting and fail to deliver genes into localized myocardial tissues. In recent years, microbubbles (MBs), used in diagnostic contrast agents for several decades, have been adapted as a vehicle for organ-specific drug, protein or gene delivery [7]. Ultrasound-targeted microbubble destruction (UTMD) provides a noninvasive, repeated, and targeted method by which transgenes can be effectively delivered to the localized cardiovascular system [8]. But yet, conventional MBs with a neutrally charged surface have a limited capacity to carry sufficient gene materials. Cationic microbubbles (CMBs) are positively charged and can improve the DNA payload on their surface, greatly facilitating gene delivery when they are combined with UTMD [9]. Studies have also indicated that CMBs may protect the bound DNA against the endonuclease degradation, resulting in an increased DNA concentration at the target site [10]. Sun et al reported that UTMD via CMBs enhances gene transfection efficiency and improves the cardiac function in the rat ischemic myocardium compared with the commercially available Definity MBs [11]. Additionally, Panje et al demonstrated that CMBs enhance UTMD-mediated gene delivery to mouse skeletal muscle relative to neutral MBs [12]. The enhancing effect of CMBs on UTMD-mediated gene delivery was, therefore, the rationale for our attempt to utilize UTMD-mediated gene delivery to inhibit HIF-1α degradation in the rat ischemic myocardium.

The gene encoding for PHD2, an oxygen-sensitive enzyme that regulates the key transcription factor HIF-1α involved in cell survival and angiogenesis, is an attractive candidate gene for cardiac gene therapy [13]. The up-regulation of hypoxia-induced HIF-1α is a major activity required for angiogenesis following ischemic injury. The key HIF-induced angiogenic genes include those encoding for vascular endothelial growth factor (VEGF), angiopoietin-2, Notch ligands, endothelial nitric oxide synthase (eNOS), and platelet-derived growth factor (PDGF) [14]. Previous studies showed that silencing PHD2 can improve cardiomyocyte viability and cardiac function after myocardial infraction (MI). Pharmacological approaches through oral administration of a PHD inhibitor (e.g., dimethyl-oxalylglycine, L-Mim, etc.) increase the microvascular density in infarcted rat hearts by stabilizing HIF-1α [15]. Direct intramyocardial injection of a short hairpin RNA (shRNA) plasmid for silencing PHD2 leads to significant improvement in angiogenesis and cardiac contractility after MI [5]. More recently, Wang et al reported that knockdown of PHD2 promotes adipose-derived stem cell (ADSC) survival and enhances their paracrine function to protect cardiomyocytes in infarcted hearts [16].

Therefore, in the present study, we attempted to synthesize a CMB to enhance UTMD-mediated gene transfection efficiency and to inhibit the HIF-1α degradation through shRNA-mediated knockdown of PHD2 for rescuing myocardial function after ischemic myocardial injury.

Materials and Methods

Preparation of the CMBs

The CMBs were prepared using the thin-film hydration and sonication method reported in previous studies (11). Briefly, 1,2-Dipalmitoyl-sn-glycero-3-phosphocholine (DPPC), 3-[N-(N',N'-dimethyl-lamino-ethane)-carbamoyl] cholesterol (DC-CHOL) and 1,2-distearoyl-sn-glycerol-3-phosphoethanolamine-N-[maleimide (polyethylene glycol)] (DSPE-PEG2000), purchased from Avanti Co., USA, were weighed and dissolved in an laboratory flask according to a certain molar proportion (10:4:1). A lipid film was formed by removing the organic solvent from the phospholipid solution with a rotary atmidometer under high vacuum. The mixture was dried under vacuum overnight. After that, phosphate-buffered saline (PBS) was added and the mixture was hydrated on a rotary evaporator, followed by sonication with octafluoropropane gas (C_3F_8) gas (Foshan Huate Gas Co. Ltd., Foshan, China). The C_3F_8 gas was bubbled through the solution for 1 minute. The mixture was then sonicated with a sonicator (20 kHz, 33-42 W). The solution of CMBs was diluted with PBS to adjust the concentration of the MBs to 1×10^9 MBs/ml. Then, the CMB solution was sterilized by ^{60}Co-γ radiation and stored at 4°C until further use.

General physical properties of the CMBs

The appropriate amount of CMBs was placed on a blood-counting chamber, and their shape and concentration were evaluated microscopically. The size distribution, concentration and zeta potential of the CMBs were measured using a Zetasizer NANO ZS system (Malvern Instruments Ltd., Malvern, UK).

Plasmid DNA purification

The pEGFP-N1 and shPHD2-EGFP (target sequence: TCGTGCCGTGCATGAACAA) plasmids were purchased from Shanghai Genechem Co. Ltd., Shanghai, China. All the plasmids were amplified from *E. coli* and purified using a plasmid DNA purification kit (Qiagen GmbH, Hilden, Germany). The DNA concentration was measured using a spectrophotometer (spectrum china) and kept at 1 μg/μl.

Assessment of plasmid binding to the CMBs

The amount of plasmid DNA bound onto CMBs was evaluated to measure the DNA loading capacity of CMBs as previously described [11]. For this assay, various doses of EGFP plasmid DNA (10, 20, 40 or 80 μg) in TE buffer were added to 5 × 10^8 CMBs and incubated for 10 min to enable DNA adsorption onto the CMBs. Then, the samples were centrifuged at 1000 × g to form two phases: an upper, milky-white layer containing the CMBs bound with DNA and a lower, clear layer containing unbound DNA. The EGFP plasmid in the lower, clear layer was collected via a second centrifugation. The unbound DNA pellet was resuspended in TE buffer to measure the DNA concentration using spectrophotometry, and the total amount of unbound DNA was obtained by multiplying by the total sample volume. All experiments were performed in triplicate. The DNA-CMB interaction was also demonstrated by laser confocal fluorescence microscopy. Forty micrograms of EGFP plasmid DNA was added to approximately 10^8 CMBs, followed by incubation and centrifugation as described above. The upper, milky-white layer was collected, stained with SYBR Gold (Life Technologies), and centrifuged at 1000 × g to form two phases. The lower layer was discarded, the upper layer was resuspended in PBS, and the rinse steps were repeated twice. Finally, the samples were diluted and imaged using fluorescence microscopy. All experiments were performed in triplicate.

Cell culture

Rat myocardial cells (H9C2) purchased from Boster Biological Engineering Co. Ltd. China, were cultured in Dulbecco's modified Eagle's medium (DMEM; Hyclone, Logan, UT, USA) supplemented with 10% fetal bovine serum, penicillin (100 U/ml) and streptomycin (100 U/ml; Life Technologies, Carlsbad, CA, USA). The H9C2 cells were cultured under normal conditions (5% CO_2, 21% O_2 and 74% N_2) in a humidified incubator at 37°C.

Ultrasound-mediated gene transfection with CMBs

H9C2 cells were seeded onto 24-well plates (Becton Dickinson, USA), and transfection experiments were performed when the cell confluence reached approximately 70%. A dose of 15 μg of plasmid per well was used throughout the study. In brief, the plasmid DNA was diluted in 300 μl Opti-MEM (Life Technologies) and mixed with 2 × 10^8/CMBs at a final volume of 500 μl to form the transfection complexes. The transfection complexes were added to the culture well and incubated for 10 minutes at room temperature. To allow contact of MBs to cells, the 24-well plate were sealed with right rubber stopper and inverted the plate. After that, cells were exposed to different ultrasound parameters through a sterile ultrasound probe placed directly onto the bottom of the 24-well plate. A Sonitron 2000 V (Nepa Gene, Co., Ltd., Chiba, Japan) was used to generate the ultrasound.

Detection of the gene transfection and cell viability

To demonstrate the efficiency of ultrasound-mediated plasmid transfection with CMBs, the experimental regimens included (i) plasmid alone (Plasmid), (ii) plasmid with ultrasound (Plasmid + Ultrasound), and (iii) plasmid with CMBs and ultrasound (Plasmid + UTMD). The H9C2 cardiac cells with CMB/DNA complexes were exposed to US under different intensities (1 MHz; duty cycle, 20%; power, 1.0, 1.5 and 2.0 W/cm2; duration, 15, 30 and 60 seconds) to identify the optimal transfection parameters for gene delivery. After gene transfection, the H9C2 cells were cultured in a medium containing 10% FBS for further 48 hours and the gene transfection was demonstrated using a FACS caliber flow cytometer (EPICS XL; Beckman Coulter Inc., Fullerton, CA, USA) with 20,000 events per sample and fluorescent microscopy. Cell viability was measured at 48 h after the transfection, using Cell Counting Kit-8 (CCK-8) according to the manufacture's protocol (Dojindo, Japan).

Assessment of cell apoptosis

To demonstrate that PHD2 silencing enhances cell survival by reducing the degradation of HIF-1α and by up-regulating the expression of angiogenic factors, an in vitro model of oxygen glucose

deprivation (OGD) was developed. The H9C2 cardiac cells under OGD were divided into three groups: (i) Control (non-transfected), (ii) EGFP (transfected with EGFP plasmid using UTMD), and (iii) shPHD2-EGFP (transfected with shPHD2-EGFP plasmid using UTMD). After transfection, the inhibition of H9C2 cell apoptosis was determined by apoptosis kit (Multi Sciences Biotech Co., Ltd.) in accordance with the manufacturer's instructions. The number of apoptotic cells was detected and analyzed using flow cytometry. The intervention outcome for PHD2 was also assessed with RT-PCR and western blot analysis. All experiments were also performed reproduced in triplicate.

Animal model

Male Sprague-Dawley rats (weight 200-220 g) were purchased from the Animal Breeding and Research Center of Tongji Medical College, Huazhong University of Science and Technology, China. The animals were housed under standard conditions of room temperature and dark-light cycles with sufficient food and water. All rats were treated according to the policy and regulations approved by Huazhong University of Science and Technology Animal Care and Use Committee. Surgical MI was induced as described previously [17]. Briefly, the rats were anesthetized with 1% pentobarbital sodium (40 mg/kg, administered intraperitoneally), intubated and ventilated with a rodent ventilator (Shanghai Yuyan Instruments, China). The left anterior descending coronary artery was ligatured with a 6/0 suture. Evidence of an MI was confirmed by S-T segment elevation and the appearance of a Q wave on an electrocardiogram. After surgery, 30 rats were randomly assigned for the transfection efficiency assay into three experimental groups: (i) plasmid alone (MI-Plasmid), (ii) plasmid with ultrasound (MI-Plasmid + US), and (iii) plasmid with CMBs and ultrasound (MI-Plasmid + UTMD). Ninety rats were randomly divided into another three groups: (i) Sham (rat chest opened/closed without ligation, untreated, n = 30 rats), (ii) MI-EGFP (MI, Ultrasonic-targeted destruction of MBs with EGFP, n = 30 rats), and (iii) MI-shPHD2-EGFP (MI, ultrasonic targeted destruction of MBs with shPHD2-EGFP, n = 30 rats) to demonstrate the shPHD2 therapeutic effect.

Gene delivery using UTMD *in vivo*

Plasmid DNA (600 μg/kg body weight, as previously reported for UTMD-mediated gene delivery to the rat myocardium) was incubated at room temperature for 20 min with CMBs (120 μl/rat) that were subsequently diluted in saline to a total volume of 500 μl/rat. At 10 minutes after ligation of the left anterior descending coronary artery, 500 μl CMB/DNA complexes were infused into the tail vein at a speed of 15 ml/h in the MI-EGFP or MI-shPHD2-EGFP rat groups. Simultaneously, an ultrasound beam was delivered with an ultrasound probe (Sonitron 2000V, Japan). Ultrasound was administered with a sonoporator using the following settings: frequency 1 MHz, duration 2 minutes, power 2.0 W/cm^2, duty cycle 50%, and probe diameter 1.2 cm. UTMD treatments were administered at 2-day intervals between Day 0 (10 minutes after MI) and Day 4. To prevent congestive heart failure due to volume overload, furosemide (0.4 mg/kg) was intramuscularly injected before the treatments in all rats. At 4 days and 28 days after operation, rats were killed and the hearts were removed for the subsequent experiment.

Analysis of green fluorescent protein expression

To confirm that the gene can be delivered into ischemic myocardial tissue, green fluorescent protein expression was analyzed. Frozen sections of myocardial tissue were prepared as described previously [18]. In brief, seven days after ultrasound irradiation, rats were killed and the heart specimens were immediately harvested. Then, the hearts were fixed in 4% paraformaldehyde overnight at 4°C, washed three times with PBS, placed in 30% sucrose overnight at 4°C to equilibrate and embedded in freezing medium Tissue Tek OCT (Sakura Finetek U.S.A., Inc. Torrance, CA, USA). For fluorescent protein expression observation, cross sections (5-μm-thick slices) were cut with a cryostat (CM1900; Leica, Wetzlar, Germany) and affixed to glass slides. The protein expression and distribution pattern were observed with an inverted Olympus IX70 microscope (Olympus Inc., Melville, NY, USA). For each sample, EGFP expression and transfection efficiency were evaluated in 6 randomly chosen fields per section and quantitated with Image-Pro Plus version 6.0 software (Media Cybernetics, Bethesda, MD) by 2 observers blinded to the conditions.

TUNEL assay

The cell apoptosis ratio in the myocardium was determined with a TUNEL assay according to the manufacturer's instructions (Roche Applied Science, South San Francisco, CA, USA). For each sample, apoptotic cardiomyocytes were evaluated in 6 randomly chosen fields per section and quantitated with Image-Pro Plus version 6.0 software (Media Cybernetics) by 2 blinded observers. The average number of TUNEL-positive cells per square millimeter (mm^2) was used for the assessment of

myocardial apoptosis.

Analysis of left ventricular function

Echocardiography was performed before (day 7) and after (week 4) the left anterior descending artery ligation. The GE vivid 7 system equipped with a 10 MHz transducer was used by an investigator blinded to group designation. The left ventricular ejection fraction (LVEF) and left ventricular fractional shortening (LVFS) were calculated by M-mode tracing. Dimension data are presented as the average of measurements of three selected beats.

Measurement of infarct size

Four weeks after the operation, rats were anesthetized with 1% pentobarbital sodium followed by cardiac perfusion with saline. The hearts were excised and washed immediately with saline to remove the excess blood before being fixed in 4% paraformaldehyde. Paraffin-embedded samples were sectioned at 6 μm, and Masson's trichrome staining was performed. The collagen volume fraction was evaluated based on the percentage of blue staining, indicative of fibrosis, and quantitated with Image-Pro Plus version 6.0 software by two observers blinded to the conditions.

Immunohistochemical analysis

Formaldehyde-fixed rat hearts were dehydrated and then embedded in paraffin. Paraffin-embedded sections (5 μm) were dewaxed and incubated with the primary antibody HIF-1α (Bioworld, catalog # BS3514), VEGF (Santa Cruz, catalog # sc-13083) or CD31 (Santa Cruz, catalog # sc-1506). After visualization with diaminobenzidine (DAB), images were acquired under the inverted Olympus IX70 microscope (Olympus Inc. Melville, NY). The CD31 immunohistochemical staining was performed to determine the capillary density. The myocardial capillary density (MCD) was also calculated as previously described [19].

Real-time polymerase chain reaction (PCR) analysis

Total RNA was extracted from treated cells or infarct myocardial tissue using TRIzol (Invitrogen, France) according to the manufacturer's protocol. Total RNA (2 μg) was reverse transcribed using an iScript cDNA synthesis kit (Bio-Rad, USA) according to the manufacturer's instructions. Quantitative real-time PCR was performed with a Bio-Rad CFX 96 Real-time Detection System (Bio-Rad). Primers for specific genes are listed in Table 1, and β-actin served as an internal reference gene. All the primers were synthesized by Shanghai Genechem Co. (Shanghai, China). The relative quantification of PHD2, HIF-1α and VEGF mRNA was determined by calculating the values of $2^{-\Delta\Delta CT}$, with each sample being normalized to the expression level of β-actin. The experiment was repeated in triplicate.

Table 1. The primer sequences of PHD2, HIF-1α, VEGF, bFGF and EPO detected by qPCR.

Genes	Primer	Sequences
β-actin	Sense	5'-GGTGCTGAGTATGTTGGAGT-3'
	Antisense	5'-CAGTCTTCTGAGTGGCAGTG-3'
PHD2	Sense	5'-TACAGGATAAACGGCCGAAC-3'
	Antisense	5'-TTGGGTTCAATGTCAGCAAA-3'
HIF-1α	Sense	5'-CGCAGTGTGGCTAC AAGAAA-3'
	Antisense	5'-TAAAT TGAACGGCCCAAAAG-3'
VEGF	Sense	5′- GCCCATGAAGTGGTGAAGTT-3′
	Antisense	5′- CTATGTGCTGGCTTTGGTGA-3′
bFGF	Sense	5′- GAACCGGTACCTGGCTATGA-3′
	Antisense	5′- ACTGCCCAGTTCGTTTCAGT-3′
EPO	Sense	5′- GAATTGATGTCGCCTCCAGA-3′
	Antisense	5′-CCAAGCCGCTCCACTCCGAACA-3′

Western blot assay

Total proteins were extracted from treated cells and myocardial infarct tissue using a RIPA buffer with protease and phosphatase inhibitors and used for western blotting as previously described [15]. The proteins' concentrations were determined with a Bradford protein assay kit (Bio-Rad, Richmond, CA, USA) using BSA as a protein standard. Proteins were separated by SDS 10% PAGE, blotted on Hybond-C membranes (Amersham Biosciences, GE Healthcare, France) and incubated with various antibodies: PHD2 (Bioworld, catalog # BS6184), HIF-1α (Bioworld, catalog # BS3514), VEGF (Santa Cruz, catalog # sc-13083), bFGF (Abcam, catalog # ab8880), caspase-3 (Santa Cruz, catalog #sc-1225) and GAPDH as an internal control (Santa Cruz, catalog # sc25778). ECL HRP Linked Rabbit IgG (Santa Cruz, catalog # sc2793) was used as the secondary antibody. The density of the respective bands was quantitated using a densitometer with AlphaView Software for FluorChem Systems (ProteinSimple™).

Statistical analysis

All results are summarized as the mean ± standard deviation (SD). ANOVA was used to evaluate statistical significances between different groups. The data were analyzed using SPSS 19.0 software. Multiple comparisons were performed through Bonferoni analysis. P values < 0.05 were considered statistically significant.

Results and discussion

Synthesis and characterization of the CMBs

The CMBs were synthesized by dissolving 1,2-dipalmitoyl-sn-glycero-3-phosphocholine (DPPC),

1,2-distearoyl-sn-glycerol-3-phosphoethanolamine-N-[maleimide (polyethylene glycol)] (DSPE-PEG2000) and 3-[N-(N',N'-dimethyl-lamino-ethane)-carbamoyl] cholesterol (DC-CHOL) in chloroform, followed by rotary evaporation to form a lipid film (Fig. 1a). After sufficient rehydration with PBS, the resulting suspension was sonicated with octafluoropropane gas (C_3F_8) and the CMBs were fabricated with a C_3F_8 gas core and a lipid shell. The concentration of CMBs was (4.09 ± 0.37) $\times 10^9$/ml. The zeta potential of the CMBs was 28.2 ± 2.21 mV. The CMBs had an average diameter of 2.59 ± 0.52 μm. The CMB properties are listed in Table 2.

Table 2. The characteristics of cationic microbubbles (CMBs).

	Concentration ($\times 10^9$/ml)	Average diameter (μm)	Zeta potential (mV)
CMB	4.09 ± 0.37	2.59 ± 0.52	28.2 ± 2.21

Plasmid DNA-binding capacity

The conjugation between plasmids and CMBs was confirmed visually by laser confocal microscopy (Fig. 1b). Green fluorescence represents successful plasmid binding onto the CMBs because SYBR Gold (Life Technologies) stains the plasmid DNA. The plasmid DNA-binding capacity of was quantified by calculating the maximum dose of plasmid DNA on the 5 × 10^8 CMBs according to the previous study [11]. As the dose of plasmid amount increased, the amount of plasmid bound to CMBs also increased. However, when the dose of plasmids climbed to 40 μg, the amount of plasmids bound to CMBs did not increase further, suggesting that the DNA binding capacity of the CMBs had reached saturation (Fig. 1c). Therefore, when 40 μg of plasmid DNA was added to the CMB solution, the amount of DNA attached to the CMBs was regarded to be the saturated DNA loading capacity for 5 × 10^8 CMBs. The saturated DNA loading amount on the CMBs was 17.81 ± 1.46 μg per 5 × 10^8 CMBs.

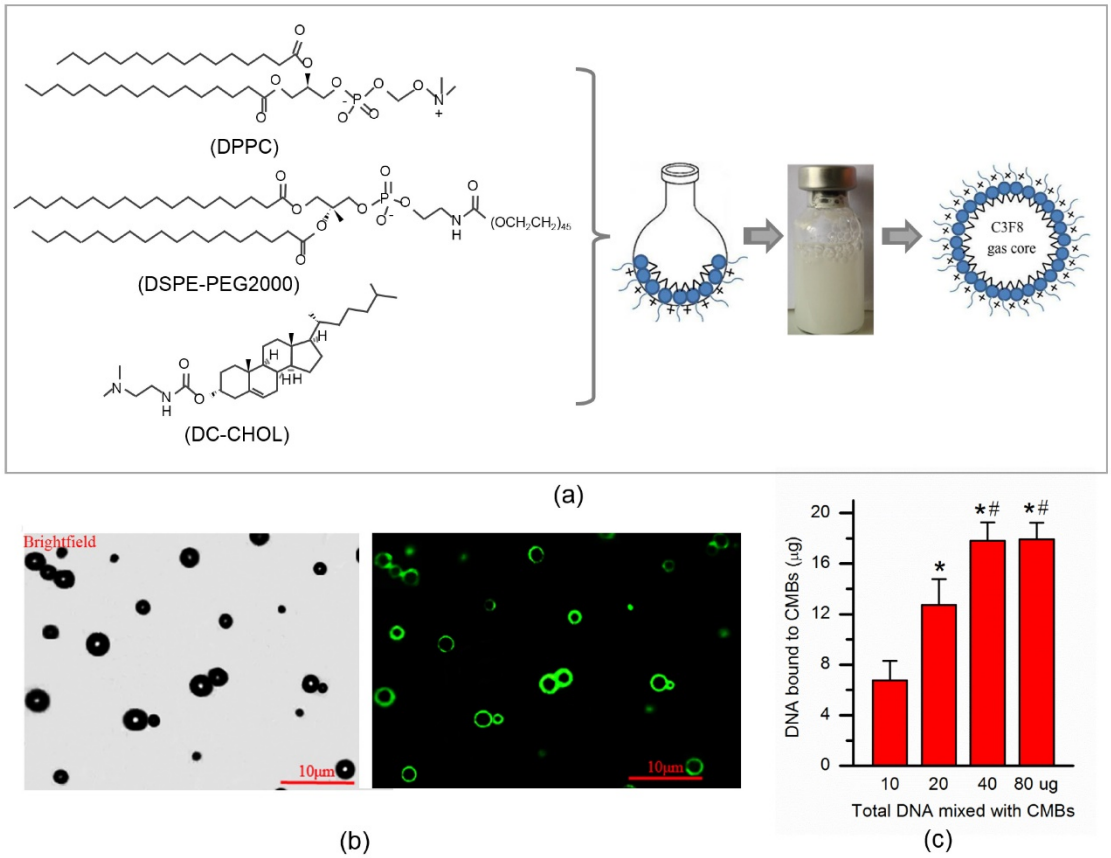

Figure 1. Fabrication and characterization of CMB. (a) Schematic illustration of the fabrication process of CMBs. 1,2-Dipalmitoyl-sn-glycero-3-phosphocholine (DPPC), 3-[N-(N',N'-dimethyl-lamino-ethane)-carbamoyl] cholesterol (DC-CHOL) and 1,2-distearoyl-sn-glycerol-3-phosphoethanolamine-N-[maleimide (polyethylene glycol)] (DSPE-PEG2000) were used to form a cationic liposome suspension, followed by rehydration with PBS. The liposome suspension was added to a vial containing octafluoropropane (C_3F_8) gas and then sonicated. The cationic microbubbles (MBs) with a C_3F_8 gas core and lipid shell were produced. (b) Bright-field of DNA-loaded CMBs and the corresponding fluorescent image. Bar, 10 μm. The plasmid DNA-binding capacity of the CMBs was quantified by calculating the maximum dose of plasmid DNA which was bound onto 5 × 10^8 CMBs. N = 6/group. *P < 0.0125 vs. 10 μg; # P < 0.0125 vs. 20 μg; & P < 0.0125 vs. 40μg.

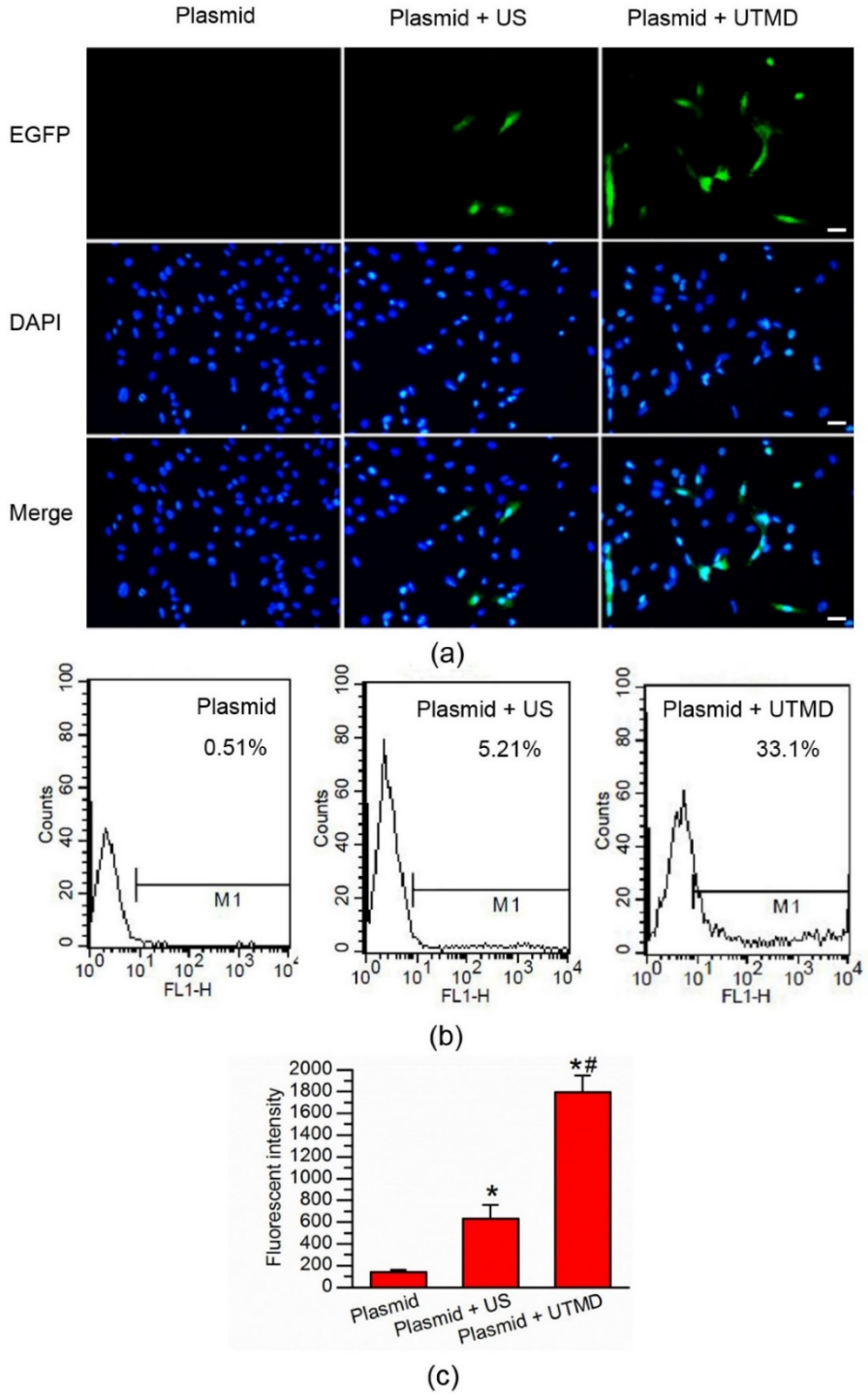

Figure 2. In vitro UTMD-mediated gene transfection of H9C2 cells. (a) Fluorescence microscopic examination of gene-transferred H9C2 cells. No GFP-positive cells were found in the EGFP-plasmid group. There were some GFP-positive cells in the plasmid + ultrasound group and significantly more GFP-positive cells in the plasmid + UTMD group. The cell nuclei were stained with DAPI. Bar, 50 μm. (b) Quantitative analysis of the transfection efficiency by flow cytometry, showing significantly higher transfection efficiency in the plasmid + UTMD group. (c) Quantitative analysis of the mean fluorescence intensity, showing significantly higher mean fluorescence intensity in the plasmid + UTMD group. US parameters: 1 MHz; duty cycle, 20%; power, 1.0 W/cm²; duration, 30 seconds. N = 6/group.*P < 0.017 vs. Plasmid; # P < 0.017 vs. Plasmid + ultrasound.

UTMD-mediated gene transfection efficiency

EGFP expression was used to determine the UTMD-mediated plasmid transfection efficiency in the H9C2 myocardial cells. A fluorescence microscope was used to observe the expression of EGFP 48 hours' post-transfection (Fig. 2a). The Plasmid only group showed nearly no green-fluorescent protein signal. Only weak green-fluorescent protein signals were noted in the H9C2 cardiac cells in the Plasmid + Ultrasound group. By contrast, the Plasmid + UTMD group displayed numerous EGFP-expressing cells. Quantitative analysis of the UTMD-mediated EGFP plasmid transfection was performed through flow

cytometry 48 hours' post-transfection (Fig. 2b). About 33.1% EGFP-positive cells were found in the Plasmid + UTMD group, significantly higher than those of the Plasmid only group (0.51%) and Plasmid + Ultrasound group (5.21%). The mean fluorescence intensity of the Plasmid + UTMD group was significantly higher than those of other two groups (Fig. 2c).

The optimal parameters for in vitro gene transfection in the H9C2 cardiac cells by UTMD were investigated. When parameters of 1 MHz, duty cycle 20%, and duration 30 seconds were fixed, the EGFP-positive cell ratio of the 1.0 W/cm² ultrasound group was significantly higher than that of any of the other 3 groups (Fig. S1a). Additionally, compared with the 1.5 or 2.0 W/cm² exposure groups, little cell damage was found in H9C2 cells treated with 1.0 W/cm² ultrasound power (Fig. S1b). Therefore, 1.0 W/cm² ultrasound power was considered a relatively satisfactory condition. When the parameters of 1 MHz, duty cycle 20%, and ultrasound power 1.0 W/cm² were fixed, the EGFP-positive cell ratio and cell viability were tested after using of different ultrasound exposure times. The EGFP-positive cell ratio of the 1.0 W/cm² ultrasound group was significantly higher than that of any of the other 3 groups (Fig. S1c). Cell damage was markedly increased in the 45 s or 60 s exposure times, whereas little cell damage was observed in cells treated with 15 s or 30 s exposure times (Fig. S1d).

UTMD-mediated shPHD2 delivery increased levels of HIF-1α and downstream angiogenic factors

To evaluate the knockdown efficiency after the delivery of shPHD2-EGFP gene into H9C2 myocardial cells, the total amounts of PHD2 mRNA and protein were determined through RT-PCR at 24 hours and western blot analysis at 72 hours after UTMD-mediated gene transfection. The PHD2 mRNA and protein levels were decreased in the shPHD2-EGFP group compared with those in the EGFP and control groups. The differences in PHD2 mRNA and protein levels between shPHD2-EGFP and the other two groups were significant (Fig. 3a, left panel; 3b, top row; and 3c, left panel).

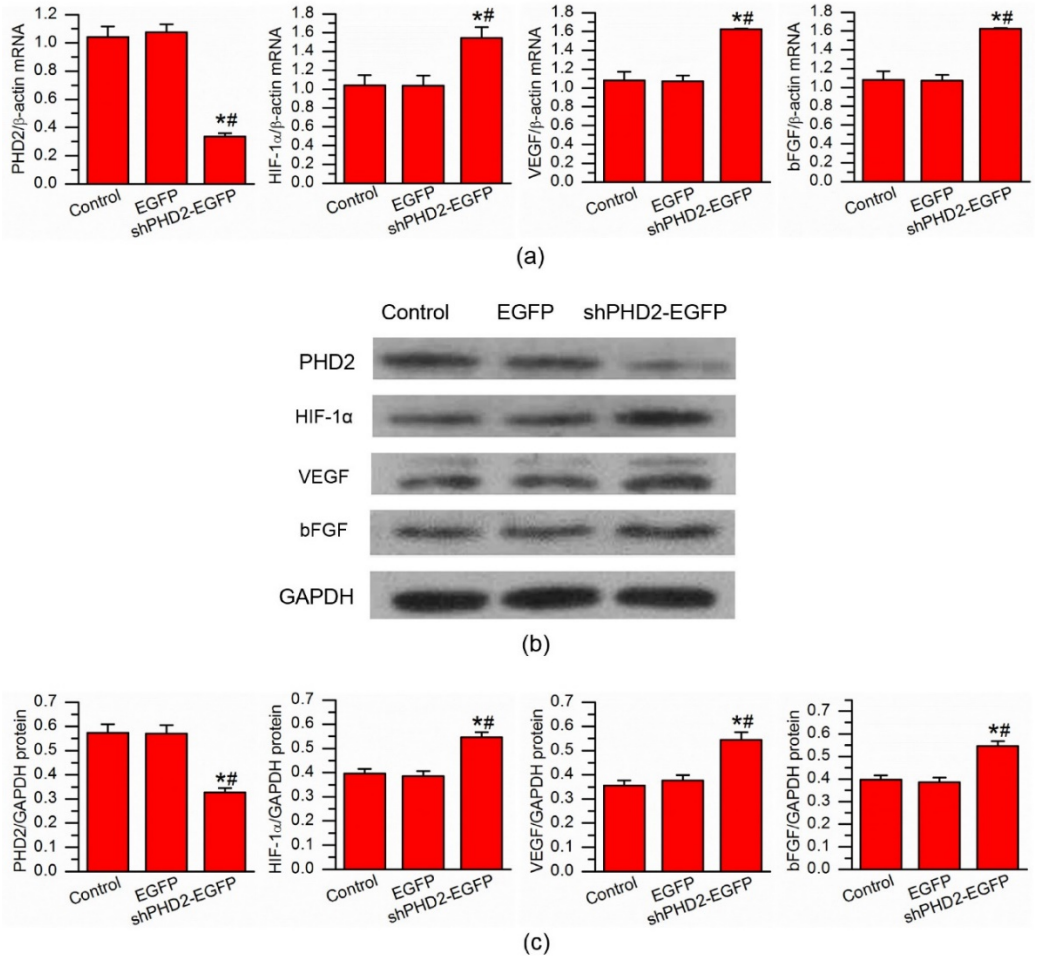

Figure 3. In vitro gene expression analysis. (a) RT-PCR analysis of the expression levels of PHD2, HIF-1α, VEGF and bFGF, demonstrating down-regulation of PHD2 and up-regulation of HIF-1α, VEGF and bFGF after UTMD-mediated shPHD2 delivery into H9C2 cells. (b) and (c) Western blotting analysis of the expression levels of PHD2, HIF-1α, VEGF and bFGF after UTMD-mediated shPHD2 delivery into H9C2 cells. There were not significant changes compared with the untreated cells with UTMD-mediated delivery of EGFP control plasmids. N = 6/group. * P < 0.017 vs. control, # P < 0.017 vs. EGFP.

These results were consistent with the results for the transfection efficiency obtained by flow cytometry, demonstrating successful down-regulation of PHD2 gene by ultrasound with shPHD2-EGFP/CMBs. To better evaluate the therapeutic effect after shPHD2-EGFP gene transfer, the mRNA and protein levels of HIF-1α and angiogenic factors VEGF and bFGF were examined. Obviously, knockdown of PHD2 resulted in an increase in the HIF-1α, VEGF and bFGF mRNA and protein levels (Fig. 3a-c), confirming the proangiogenic effects of shPHD2 treatment.

Silencing of PHD2 reduced H9C2 cell apoptosis via a HIF-1α-dependent pathway

The H9C2 cell apoptosis after ultrasound-mediated shPHD2 delivery was evaluated quantitatively by flow cytometry and by western blot analysis. The results were shown in Fig. 4. Treatment with OGD increased the amount of activated caspase-3 and Annexin V-PE/7-AAD-positive cells in H9C2 cells. Delivery of shPHD2-EGFP but not EGFP significantly decreased the percentage of apoptotic cells and the amount of cleaved caspase-3 (Fig. 4a-d).

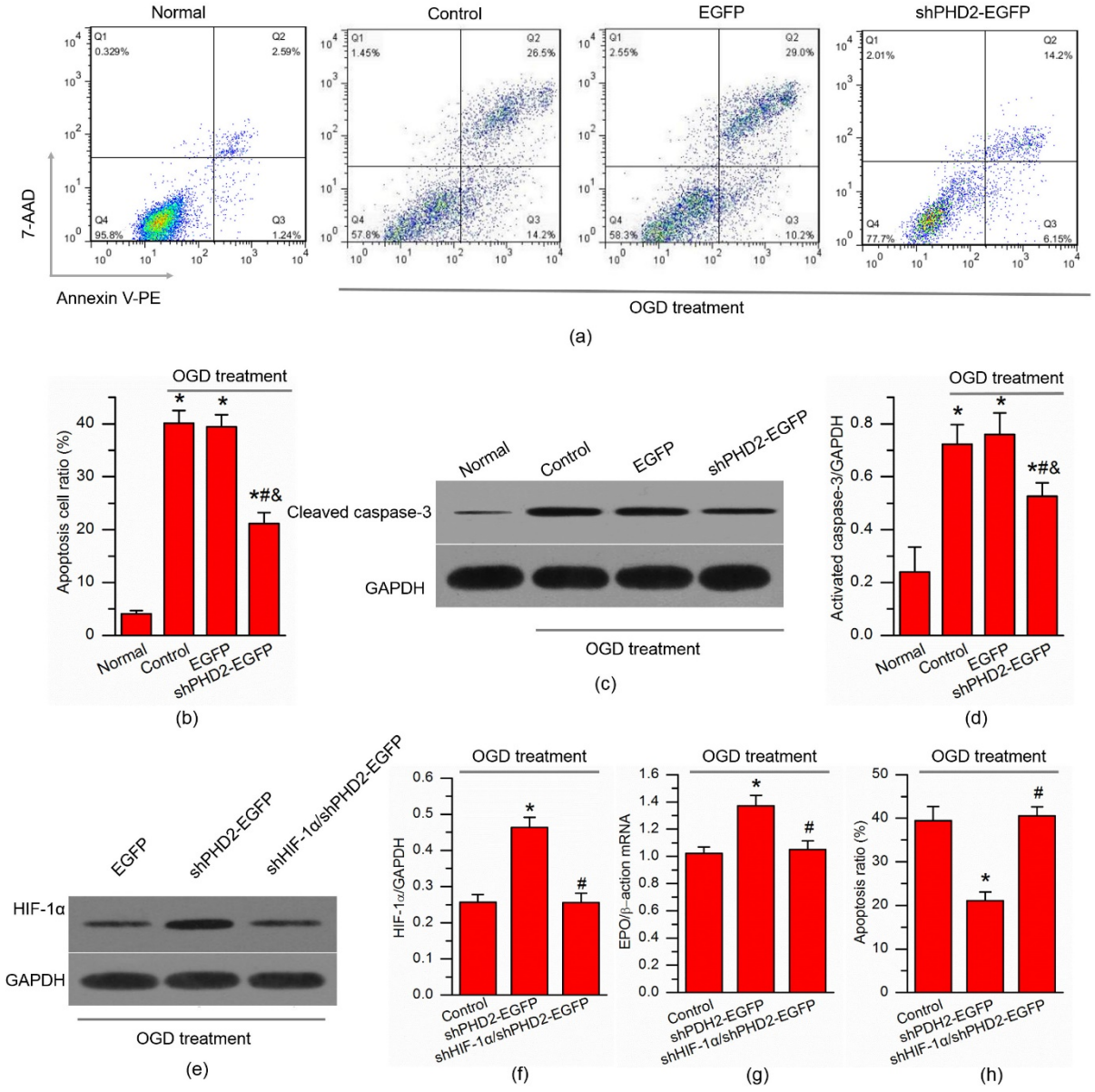

Figure 4. Knockdown of PHD2 reduced H9C2 cell apoptosis through HIF-1α-dependent pathway. (a) Flow cytometry analysis of H9C2 cell apoptosis after Annexin V-PE/7-AAD double staining. H9C2 cell apoptosis was induced by oxygen glucose deprivation (OGD) for 6 hours, followed by UTMD-mediated delivery of EGFP control or shPHD2 plasmids. (b) Quantitative analysis of the ratios of H9C2 cell apoptosis. N = 6. * P < 0.0125 vs. Normal; # P < 0.0125 vs. Control; & P < 0.0125 vs. EGFP. (c) Western blotting analysis of cleaved caspase-3 expression in H9C2 cells and (d) the signal intensities from these blots. N = 6. * P < 0.0125 vs. Normal; # P < 0.0125 vs. Control; & P < 0.0125 vs. EGFP. (e) Western blotting analysis of HIF-1α expression in H9C2 cells and (f) the signal intensities from these blots. (g) qPCR assay of the mRNA expression of canonical HIF downstream target EPO in H9C2 cells. (h) Apoptotic inhibition capability was lost after H9C2 cells transfected with shPHD2 and shHIF-1α. The apoptotic cell ratios were detected by flow cytometry after Annexin V-PE/7-AAD double staining. N = 6/group. * P < 0.017 vs. EGFP; # P < 0.017 vs. shPHD2-EGFP.

In order to confirm the decrease of H9C2 cell apoptosis induced by PHD2 knockdown via a HIF-1α-dependent pathway, HIF-1α and its downstream target EPO were detected. As expected, HIF-1α protein level was increased significantly by shPHD2-EGFP treatment compared with that after EGFP treatment in the presence of OGD (Fig. 4e-f). Concomitantly, the mRNA levels of canonical HIF downstream target EPO were also significantly increased by shPHD2-EGFP treatment (Fig. 4g). More importantly, the increases of both HIF-1α proteins and HIF-1α target mRNAs (EPO) in the shPHD2-EGFP treated group could be reduced by shHIF-1α treatment. When HIF-1α was silenced in H9C2 cells, the anti-apoptotic effect of shPHD2 on H9C2 cells was lost (Fig. 4h).

In vivo ultrasound imaging and gene transfection by UTMD

As was shown in the Fig. S2, there was not the ultrasound imaging signals in the M-mode before injection of CMB/DNA complexes. In contrast, the ultrasound imaging signals could be obviously observed after injection of CMB/DNA complexes. Four days after UTMD, EGFP expression in the hearts of rats that received the CMB solution containing the EGFP gene confirmed the successful in vivo transfection using the UTMD technique. EGFP expression at the infarct and peri-infarct myocardial tissues was examined under fluorescence microscopy on the fourth day after UTMD. The data were presented in Fig. 5. Obviously, no EGFP expression was found in the Plasmid group. Only a few myocardial cells expressing EGFP were detected in the Plasmid + US groups while they were significantly increased in the Plasmid + UTMD group ($P < 0.05$). This finding indicated the successful in vivo gene transfection into myocardial tissue using the UTMD technique.

To confirm the effects of shPHD2 gene delivered to the myocardium, the total amount of PHD2 mRNA and protein in the scar and border zone (combined) was determined by RT-PCR and western blot analysis, respectively. At 4 days following UTMD-mediated shPHD2 plasmid delivery, the PHD2 mRNA levels in the scar/border zone of the myocardium were significantly decreased in rats receiving the shPHD2-EGFP plasmid compared with rats receiving the EGFP plasmid. Also, the mRNA levels of HIF-1α and angiogenic factors VEGF and bFGF were significantly increased in the MI-shPHD2-EGFP group compared with those in the MI-EGFP group (Fig. S3a). Similar changes of protein expression levels for (PHD2, HIF-1α, VEGF and bFGF) also found (Fig. S3b and S3c), indicating the possible angiogenesis effects of UTMD-mediated shPHD2 gene localized delivery in vivo.

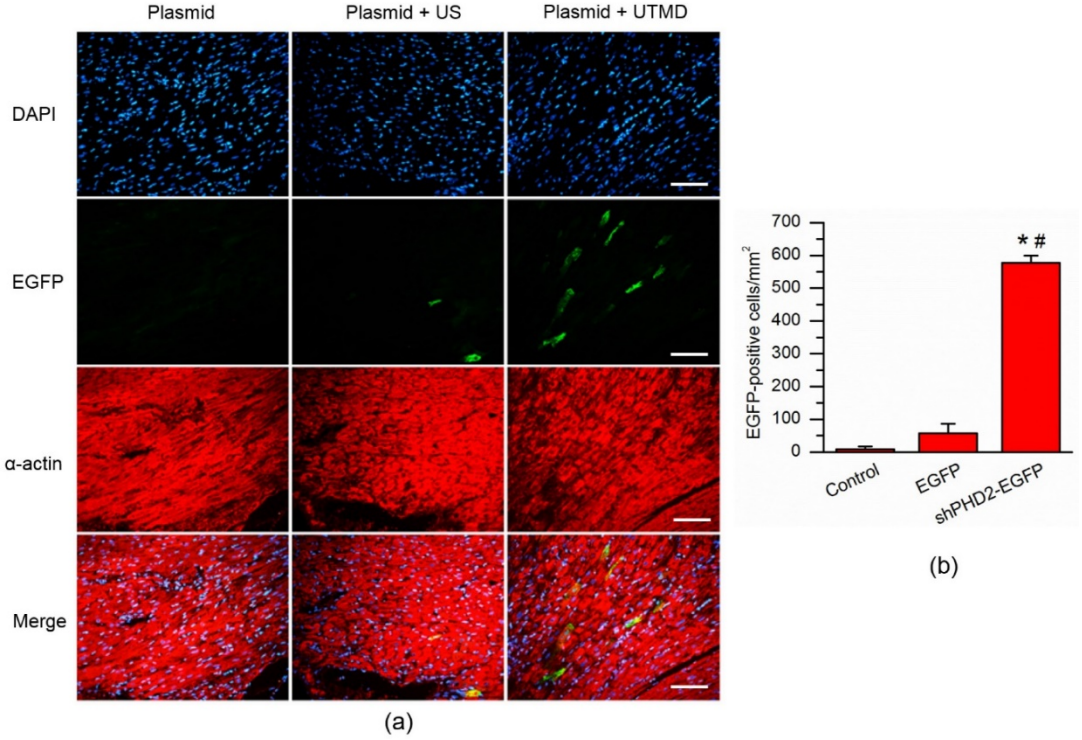

Figure 5. Fluorescence micrograph of cardiomyocytes on the infarct border area after UTMD-mediated gene delivery. (a) Cardiomyocytes that received only plasmid showed no fluorescence cells within the infarct border area. A few EGFP-positive cells could be found in the cardiomyocytes received plasmid and ultrasound. By contrary, numerous EGFP-positive cells were observed in the cardiomyocytes received plasmid and UTMD. Cardiomycytes were labelled by immunofluorescent histochemical staining with anti-α-actin antibody. The cell nuclei were stained with DAPI. Bar, 50 μm. (b) Quantitative analysis of the EGFP-positive cell ratios in the gene transfection cardiomyocytes. N = 10/group. * $P < 0.017$ vs. Plasmid; # $P < 0.017$ vs. Plasmid + Ultrasound.

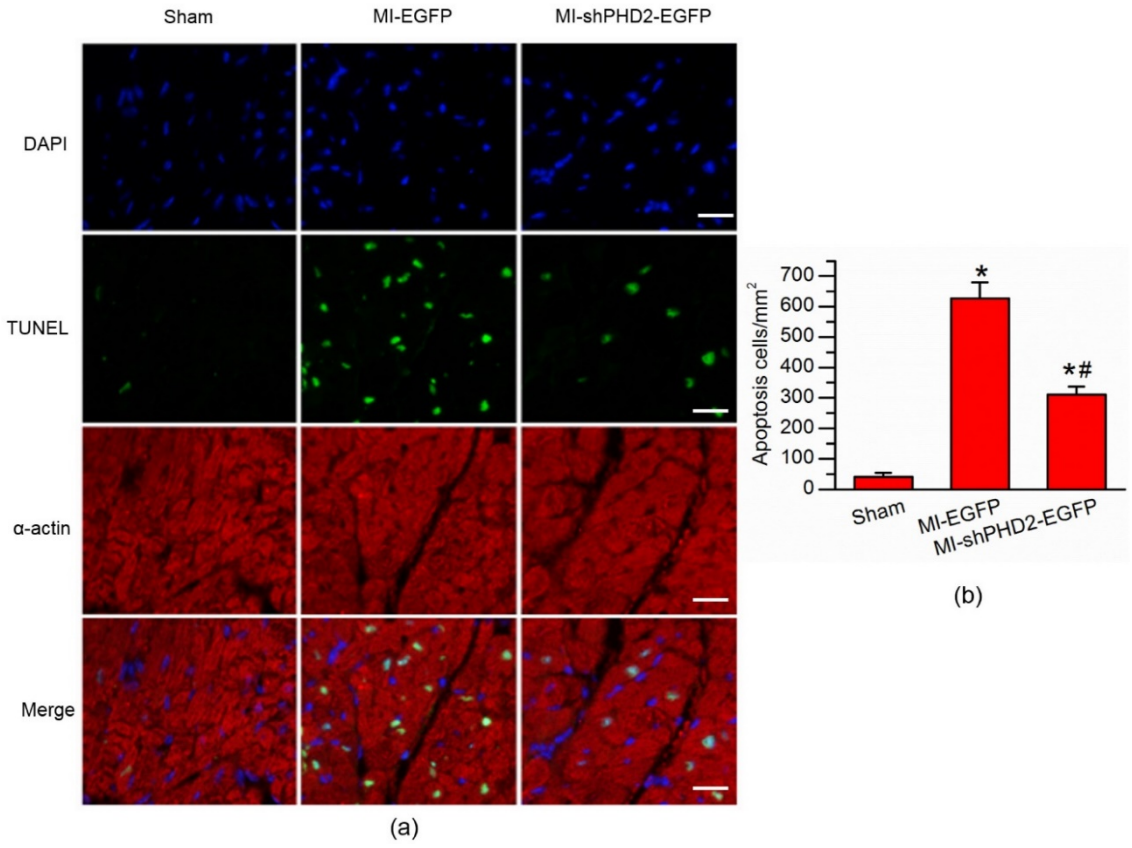

Figure 6. PHD2 silencing reduced cardiomyocyte apoptosis. (a) TUNEL assay was used for detection of cardiomyocyte apoptosis from Sham, UTMD-mediated EGFP or shPHD2 delivery. Significantly less apoptotic cells were found in the shPHD2-treated cardiomyocytes in infarct border zone at 48 hours post-MI. Cardiomyocytes were labelled with anti-α-actin antibody. The cell nuclei were stained with DAPI. Bar, 20 μm. (b) Quantitative analysis of the apoptotic cell ratios by counting the number of positive cells per square micrometer area in the gene transfection cardiomyocytes. N = 10/group. * $P < 0.017$ vs. Sham; # $P < 0.017$ vs. MI-EGFP.

Ultrasound contrast imaging was used to examine microvascular flow after inhibition of PHD2. Compared with the Sham and MI-EGFP group, there was a significant increased myocardial perfusion to be observed in the infarction area (arrows) in the MI-shPHD2-EGFP group (Fig. S4a). The contrast agent signal intensity of the anterior wall and posterior wall were measured by QLAB (Fig. S4b), demonstrating a significantly improved in the MI-shPHD2-EGFP group than that of the MI-EGFP group ($P < 0.017$) (Fig. S4c).

Effect of shPHD2 delivery on post-MI myocardial remodeling

The impact of UTMD-mediated shPHD2 transfection on myocardial protective effects at 48 hours post-MI was evaluated with a TUNEL assay, by which the amount of apoptotic cells in the infarct border zone was measured. As shown in Fig. 6, the percentage of TUNEL+ cardiomyocyte nuclei was more significantly reduced in shPHD2-EGFP-treated hearts compared with EGFP-treated hearts.

Increased cardiac function and improved infarct morphology after UTMD-mediated shPHD2 delivery

Cardiac function was determined by echocardiographic examination (Fig. 7a). LVFS and LVEF were similar among all groups before surgery (prior to gene delivery; Fig. 7b-c; $P > 0.017$). At 4 weeks after gene delivery by UTMD, LVFS and LVEF were significantly higher in the rats receiving UTMD-mediated delivery of shPHD2 plasmid than in those receiving the EGFP plasmid (Fig. 7b-c; $P < 0.017$).

Histological examination of the rat hearts was performed at 4 weeks after gene therapy. The staining of the myocardial sections with Masson's trichrome revealed less fibrosis and scar tissue but more viable tissue within the infarct region in the MI-shPHD2-EGFP group (Fig. 8a). The scar area of the infarcted myocardium was smaller after UTMD-mediated shPHD2-EGFP plasmid delivery than that of the MI-EGFP group (Fig. 8b; $P < 0.017$). These data demonstrated that UTMD-mediated localized myocardial delivery of shPHD2 plasmids prevented the heart from infarction, and thus improved cardiac function.

Effect of UTMD-mediated shPHD2 transfection on post-ischemic neovascularization

Since the decrease in PHD2 activity was associated with HIF-1α accumulation, we assessed the HIF-1α expression via immunohistochemical staining. Expression of HIF-1α was significantly increased in the MI-shPHD2-EGFP group compared to the MI-EGFP group (Fig. 9a; $P < 0.05$). To further analyze the effect of PHD2 silencing and subsequent HIF-1α up-regulation on HIF-1α-dependent proangiogenic factors, we analyzed the expression of VEGF as well. Similarly, VEGF-positive staining cells were also increased in the MI-shPHD2-EGFP group compared to the MI-EGFP group (Fig. 9b; $P < 0.05$). Also, immunohistochemical staining for CD31 was used to analyze the effect of shPHD2 on the myocardium capillary density. More CD31-positive staining cells were detected in the MI-shPHD2-EGFP group compared to the MI-EGFP group (Fig. 9c; $P < 0.05$).

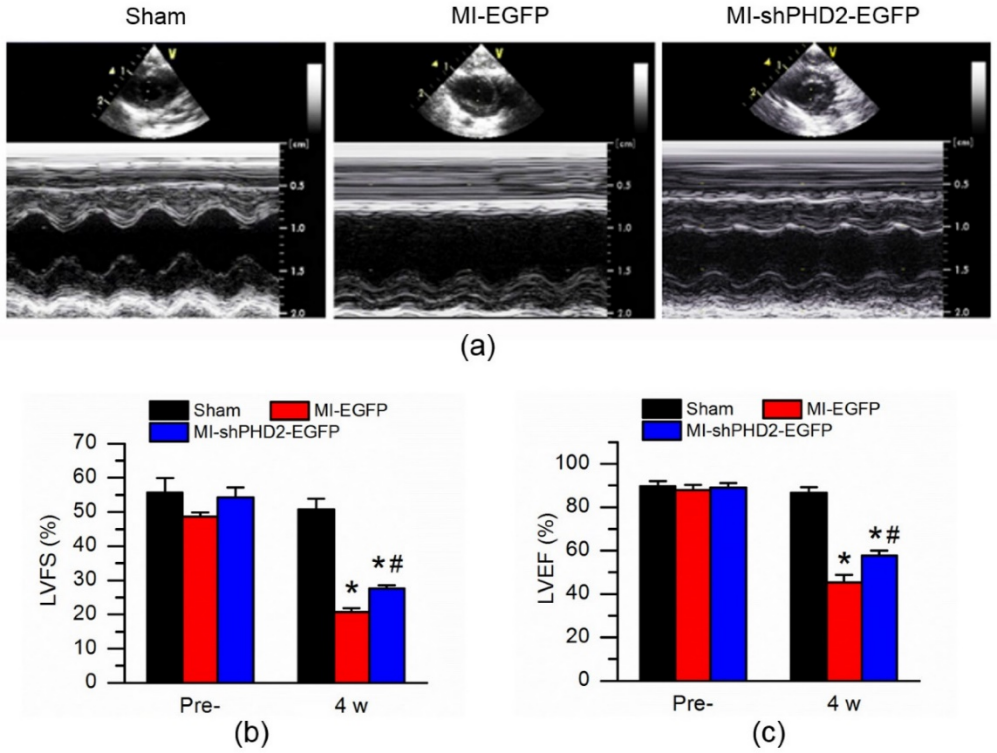

Figure 7. Cardiac function improvement after PHD2 silencing in MI rat. (a) Representative M-mode images of hearts with sham surgery or MI at 4 weeks after UTMD-mediated EGFP or shPHD2-EGFP delivery. (b) Left ventricle ejection fraction (LVFS) and (c) left ventricle fractional shortening (LVEF) were determined at 4 weeks N = 10/group. * $P < 0.017$ vs. Sham; # $P < 0.017$ vs. MI-EGFP.

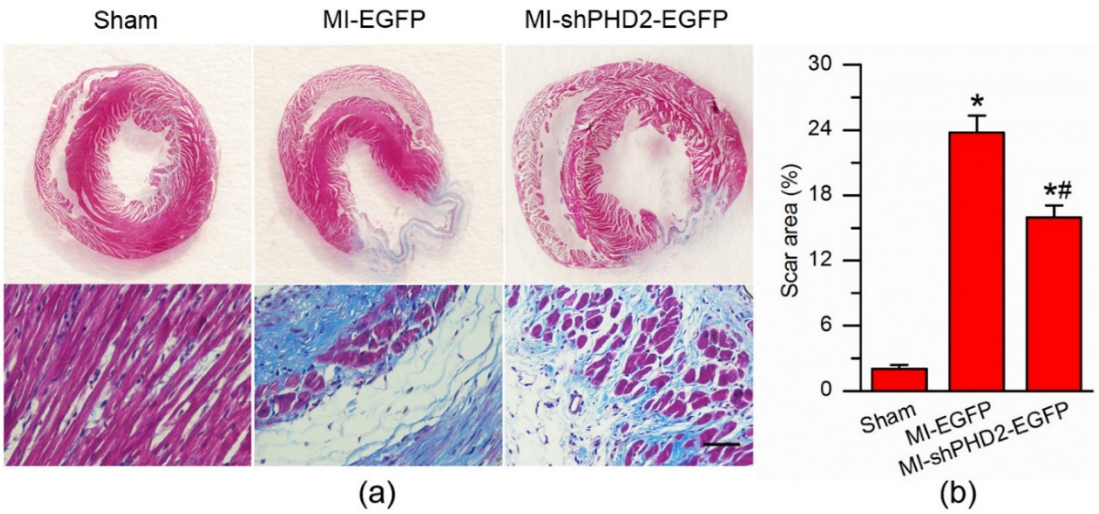

Figure 8. Infarct size and cardiomyocyte fibrosis after PHD2 silencing. (a) Representative Masson's trichrome-stained histological sections from Sham, UTMD-mediated EGFP or shPHD2 delivery groups at 4 weeks. Bar, 50 μm. (b) The infarct size, expressed as a percentage of the total tissue area, was significantly attenuated in the UTMD-mediated shPHD2-EGFP group compared with UTMD-mediated EGFP group. N = 10/group. * $P < 0.017$ vs. Sham; # $P < 0.017$ vs. MI-EGFP.

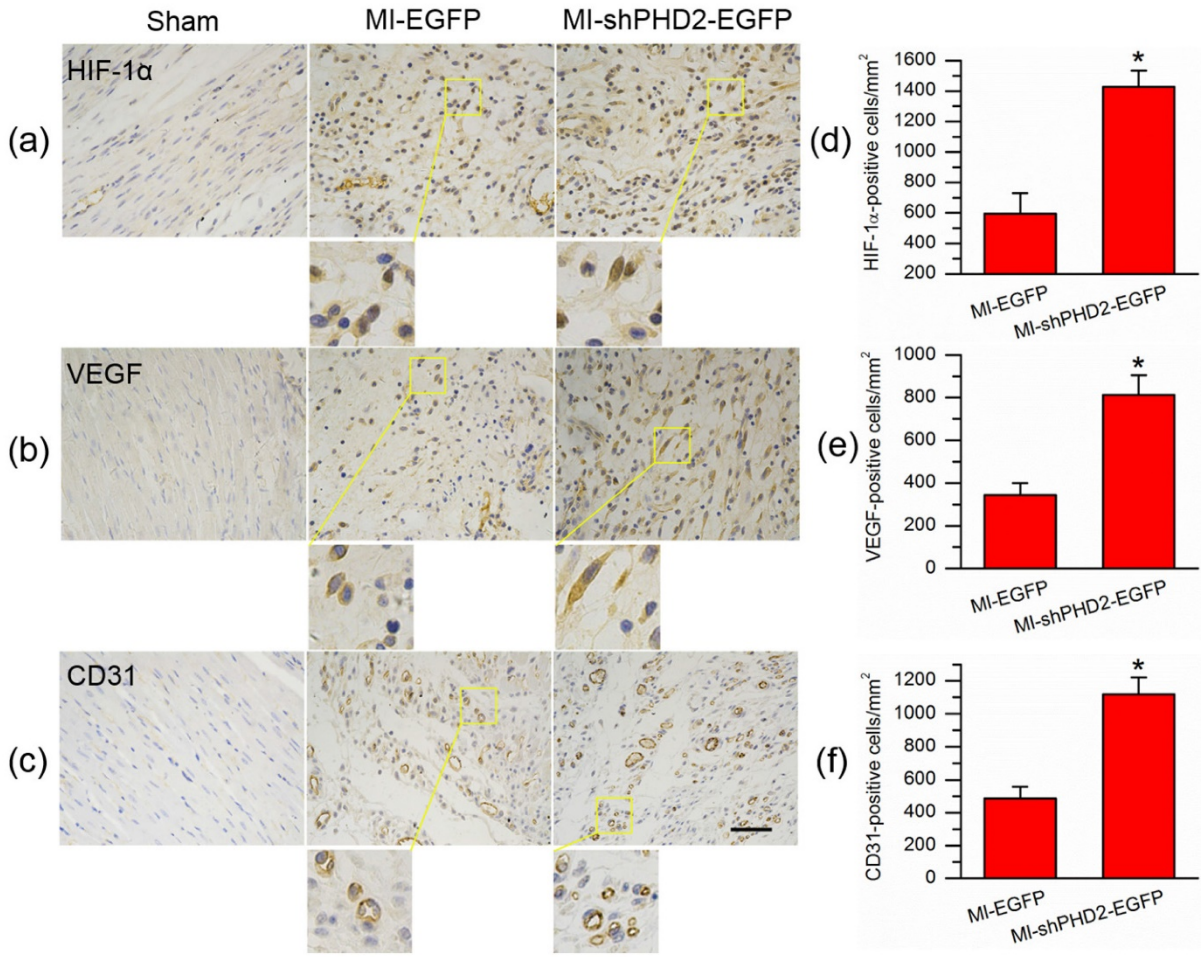

Figure 9. UTMD-mediated shPHD2 delivery increased neovascularization through HIF-1α-dependent pathway. (a)-(c) Immunohistochemical staining assay detected HIF-1α-, VEGF-, and CD31-positive cells in the infarct area from in the Sham, EGFP- and shPHD2-treated groups on day 28 after ultrasound irradiation. There was significantly more positively stained cells in the UTMD-mediated shPHD2-treated myocardia, indicating HIF-1α-dependent neovascularization after UTMD-mediated shPHD2 delivery. (d)-(f) Quantitative analysis of the protein expression levels by counting the number of positive cells per square micrometer area in the gene transfection cardiomyocytes. N = 10/group. * $P < 0.05$ vs. MI-EGFP.

Discussion

In this study, we applied a novel gene delivery method, UTMD combined with CMBs, to transfer shPHD2 into rat myocardial cells (H9C2) and ischemic myocardia. The important findings can be summarized as follows: (1) The CMBs exhibited a significantly increased DNA-binding capacity due to their high positive potential, achieving 17.81 ± 1.46 μg of DNA loading amount per 5 × 10^8 CMBs. (2) The transfection efficiency of plasmid DNA was markedly improved by UTMD combined with CMBs in the both in vitro and in vivo conditions. (3) shPHD2 transfection by UTMD can effectively down-regulate the PHD2 gene and activate the expression of downstream angiogenic genes involved in the hypoxia response pathway. (4) Localized myocardial delivery of shPHD2 by UTMD can enhance neoangiogenesis, reduce myocardial apoptosis, and thus improve ventricular function in a rat model of myocardial infarction during a 4-week follow-up.

The therapeutic use of a transgene relies on the capacity of the targeted gene to be expressed over the long term in the appropriate target tissue. Previous studies have demonstrated that the gene transfection efficiency was modest using ultrasound-mediated gene delivery with neutral MBs [20, 21]. In spite of this, UTMD has many advantages, such as noninvasiveness, repeatability and targeted gene delivery into some localized tissues [22, 23]. Therefore, UTMD has been continuously investigated since its development. If its modest transfection efficiency can be overcome, UTMD as a non-viral transfection system may make clinical gene therapy a reality. Currently, the main challenge with this approach is how to improve the transfection efficiency. According to previous studies that cationic liposomes could mediate gene transfection, CMBs were developed to enhance the loading capacity of DNA. Conventionally, CMBs were prepared through integrating different types of cationic lipids, such as DMTMP, DSTAP, DOTAP, DPTAP, DOTMA, DDAB

or Stearic-PEI600, into the lipid microbubble shell. Then, the loading capacity was augmented through charge coupling, and the transfection efficiency was also increased compared with neutral microbubbles [9, 11, 24, 25, 26, 27]. Unlike the previous CMBs, the present study reports the synthesis of CMBs using DPPC, DC-CHOL and DSPE-PEG2000, as shown in Fig. 1. In contrast to other reports, DC-Chol was selected in our study to provide the positive charged potentials on the surface of the MBs. In fact, this lipid is one of the most efficient and commonly used cationic lipids and has been widely used in gene transfection and drug delivery [28]. In our experiment, the CMBs were prepared by adding a specific molar ratio of DC-Chol to DPPC to DSPE-PEG2000, producing 28.2 ± 2.21 mV of the mean zeta potential of the CMBs (Table 2). The CMBs were stable in solution for one month at 4°C. The stability of the CMBs decreased with increasing amounts of DC-Chol, in accordance with a previous report [10], although some studies failed to note that the zeta potential affected the stability of MBs. Here, we tested the idea that the CMBs could combine with plasmid (Fig. 1b), and found that the plasmid loading capacity of the CMBs was slightly higher than those demonstrated in some reports [29]. Moreover, the combination capacity of the plasmid reached saturation with an increasing amount of plasmid when the number of CMBs was fixed in our experiments (Fig. 1c). Some studies have suggested that the plasmid loading capacity of a CMB can be saturated, which is in concordance with our findings [10]. Sun et al [11] reported no saturation for the plasmid combining capacity, even when 80 μg of plasmid was added; however, they did not describe the number of CMBs used in their experiments. The zeta potentials, plasmid loading capacities and transfection efficiencies of CMBs reported by previous researchers have varied. Therefore, further investigation regarding the relationships between the zeta potential, plasmid loading capacity and transfection efficiency of CMB is still required.

The previous studies revealed a significant increase in transfection efficiency by only ultrasound [30, 31, 32]. However, the transfection efficiency using ultrasound was still not sufficiently high to meet the treatment demand. Combined with MBs, ultrasound exposure markedly increased the gene transfection efficiency in previous experiments [33, 34, 35]. In the present experiment, we showed that the number of EGFP-labeled H9C2 cells in the Plasmid + UTMD group was significantly greater than in the Plasmid or the Plasmid + Ultrasound groups (Fig. 2), which demonstrated that UTMD has a greater capability to increase plasmid gene delivery to H9C2 cardiac cells. Transgene expression is increased due to the formation of transient holes in the cell membrane resulting from the destruction of MBs [35, 36]. The presence of ultrasound contrast agents can greatly reduce the threshold of acoustic cavitation production, resulting in the improvement in transfection efficiency by UTMD [37, 38, 39]. Our in vivo data also confirmed that UTMD was potentially effective in plasmid gene delivery. The combination of ultrasound with CMBs exhibited a marked increase in EGFP expression in the myocardium. Most documents supported that interstitial capillary permeability was increased by UTMD, facilitating plasmid gene delivery to the target tissue. Indeed, UTMD has been reported to cause microvessel rupture and change blood vessel wall permeability, resulting in the extravasation of polymer microspheres into the parenchyma [40, 41, 42, 43]. In the present study, the CMBs consisting of gas-filled microspheres surrounded by a cationic lipid shell of DPPC, DC-CHOL and DSPE-PEG2000 are different from other conventional contrast agents. We proved the CMBs can effectively enhance DNA-binding capacity and may further improve gene transfection efficiency.

Theoretically, ultrasonic irradiation in combination MBs can promote gene delivery into target cells and tissues. In fact, different exposure modalities may be associated with different levels of transfection efficacy [34, 44, 45]. Plasmid delivery using UTMD is associated with many factors. As shown in Fig. S1, the optimal irradiation parameters with an acoustic intensity of 1.0 W/cm^2 and an exposure time of 30 seconds were optimized for our in vitro gene delivery study. The transfection efficiency reached a maximum at the optimal supersonic irradiation conditions. Therefore, we used this parameter in the vitro experiment. These data indicate that optimal parameters for naked gene transfection using UTMD are important.

Recently, a novel therapeutic approach for delivering potent angiogenic factors to expedite and/or augment new vessel growth has been applied to treat ischemic diseases. A number of angiogenic growth factors, such as VEGF, FGF, IGF and a transcription factor for angiogenesis, hypoxia-inducible factor (HIF), have been reported to use for restoring cardiac function after an MI [5, 46, 47]. Recently HIF-1α has received great attention because this transcription factor controls the expression of over 60 genes that affect cell survival and metabolism in adverse conditions, including VEGF, FGF, IGF, erythropoietin, nitric oxide synthase, and others [48]. HIF-1α has a short half-life of only approximately 5 minutes due to hydroxylation by

PHD2 under normoxia [49]. The activity of PHD2 decreases under hypoxia, which results in less hydroxylation and accumulation of HIF-1α [50]. However, reoxygenation easily restores HIF-1α degradation due to the increased PHD2, which blocks the cytoprotection of HIF-1α [51]. The silencing of gene expression by RNA interference is a powerful tool for disease therapy. In this study, PHD2 was selected as the knockdown target. Therefore, we synthesized shRNA to knockdown PHD2. To determine the gene-silencing effect of shPHD2 after its transfection by UTMD, the expression of PHD2 was quantified by RT-PCR and western blot analysis. In the in vitro experiment, we found that the CMB-assisted mediation of shPHD2 by ultrasound pulses could inhibit PHD2 gene expression. As expected, CMB-assisted shPHD2 delivery with ultrasound also increased the levels of HIF-1α and its downstream angiogenic factors VEGF and bFGF in H9C2 cardiac cells, as shown in Fig. 3. In addition, the in vivo data confirmed that UTMD could directly deliver the shPHD2 gene to the myocardium in the rat MI model, resulting in lower PHD2 mRNA and protein expression in the shPHD2 group than in the other two groups. Likewise, the results of the mRNA and western blot analysis showed increased myocardial levels of HIF-1α and its downstream angiogenic factors VEGF and bFGF in the shPHD2-EGFP group in comparison with other two groups (Fig. S3). Ultrasound in combination with CMBs and shPHD2 yielded the strongest gene down-regulation, consistent with previous reports [5, 51]. HIF-1 activates the transcription of genes whose protein products may inhibit apoptosis in response to hypoxia/ischemia, including EPO, Cardiotrophin-1 (CT-1) and VEGF [52, 53, 54]. We believe that silencing PHD2 is able to inhibit cell apoptosis under OGD. In this study, we investigated whether shPHD2 transfection with UTMD could inhibit H9C2 cardiac cells in vitro and myocardial apoptosis in vivo. As shown in Fig. 4, after gene transfection using UTMD in vitro, the apoptotic cell ratio in the control and EGFP groups was elevated, whereas apoptosis was dramatically decreased after shPHD2-EGFP transfection with UTMD. We observed the same phenomenon in vivo in myocardia treated with a mixture of CMBs and shPHD2 followed by ultrasound irradiation. We suggest that silencing of PHD2 significantly increases HIF-1α abundance, thereby inhibiting myocardial apoptosis in the injured heart in vivo. Given the efficient transfection of tail vein plasmid DNA injection using ultrasound with CMBs, we finally examined the activity of angiogenesis in a rat MI model. As shown in Fig. 8, Fig. 9 and Fig.S4, decrease of the infarcted scar size and left ventricular interstitial fibrosis and increase of the capillary density and myocardial perfusion were demonstrated in the in vivo rats transfected with shPHD2-EGFP compared to EGFP plasmid. These results indicate that our approach may be beneficial for the inhibition of ventricular remodeling and improvement of heart function (Fig. 7), which are consistent with the findings of the previous study [5]. Therefore, we believe that the UTMD-mediated shRNA plasmid technique, as a promising method for targeted delivery of a gene to cardiac tissue, can successfully mediate PHD2 silencing, inhibit ventricular remodeling and improve heart function in vivo.

Conclusions

Our study applied CMBs to inhibit HIF-1α degradation via PHD2 shRNA knockdown using UTMD. We demonstrated that ultrasound-mediated gene delivery with CMBs enhanced shPHD2 gene transfection and led to significant improvement in angiogenesis and contractility in myocardial ischemic heart disease in rats. The combined utilization of UTMD and CMBs to cardiac gene transfection provides a potential therapy for ischemic myocardial injury.

Supplementary Material

Supplementary figures.
http://www.thno.org/v07p0051s1.pdf

Acknowledgements

The work was supported by National Key Basic Research Program of China (973 Program) (Grant Nos. 2015CB755500, 2013CB733800), National Natural Science Foundation of China (Grant Nos. 81671705, 81471678, 81271582, 81301235, 81571701, 81371563, 11325420, 11534013), Shenzhen Science and Technology Innovation Committee grants (JCYJ20150521144321010 and ZDSYS20140509162754023).

Competing Interests

All the authors declare they have no competing of interests.

References

1. Yellon DM, Hausenloy DJ. Myocardial reperfusion injury. N Engl J Med. 2007; 357(11):1121-35.
2. Shimokawa H, Yasuda S. Myocardial ischemia: current concepts and future perspectives. J Cardiol. 2008; 52(2): 67-78.
3. Semenza GL. Hypoxia-inducible factor 1 and cardiovascular disease. Annu Rev Physiol. 2014; 76: 39-56.
4. Lee JW, Bae SH, Jeong JW, Kim SH, Kim KW. Hypoxia-inducible factor (HIF-1) alpha: its protein stability and biological functions. Exp Mol Med. 2004; 36(1): 1-12.
5. Huang M, Chan DA, Jia F, et al. Short hairpin RNA interference therapy for ischemic heart disease. Circulation. 2008; 118(14 Suppl): S226-33.

6. Müller OJ, Katus HA, Bekeredjian RHA, et al. Targeting the heart with gene therapy-optimized gene delivery methods. Cardiovasc Res. 2007; 73(3): 453-62.
7. Bekeredjian R, Grayburn PA, Shohet RV. Use of ultrasound contrast agents for gene or drug delivery in cardiovascular medicine. J Am Coll Cardiol. 2005; 45(3): 329-35.
8. Mayer CR, Bekeredjian R. Ultrasonic gene and drug delivery to the cardiovascular system. Adv Drug Deliv Rev. 2008; 60(10): 1177-92.
9. Wang DS, Panje C, Pysz MA, et al. Cationic versus neutral microbubbles for ultrasound-mediated gene delivery in cancer. Radiology. 2012; 264(3): 721-32.
10. Zhou Y, Gu H, Xu Y, et al. Targeted Antiangiogenesis Gene Therapy Using Targeted Cationic Microbubbles Conjugated with CD105 Antibody Compared with Untargeted Cationic and Neutral Microbubbles. Theranostics. 2015; 5(4): 399-417.
11. Sun L, Huang CW, Wu J, et al. The use of cationic microbubbles to improve ultrasound-targeted gene delivery to the ischemic myocardium. Biomaterials. 2013; 34(8): 2107-16.
12. Panje CM, Wang DS, Pysz MA, et al. Ultrasound-mediated gene delivery with cationic versus neutral microbubbles: effect of DNA and microbubble dose on in vivo transfection efficiency. Theranostics. 2012; 2(11): 1078-91.
13. Loinard C, Ginouvès A, Vilar J, et al. Inhibition of prolyl hydroxylase domain proteins promotes therapeutic revascularization. Circulation. 2009; 120(1): 50-9.
14. Semenza GL. Targeting HIF-1 for cancer therapy. Nat Rev Cancer. 2003; 3(10): 721-32.
15. Milkiewicz M, Pugh CW, Egginton S. Inhibition of endogenous HIF inactivation induces angiogenesis in ischaemic skeletal muscles of mice. J Physiol. 2004; 560(Pt 1): 21-6.
16. Wang WE, Yang D, Li L,et al. Prolyl hydroxylase domain protein 2 silencing enhances the survival and paracrine function of transplanted adipose-derived stem cells in infarcted myocardium. Circ Res. 2013; 113(3): 288-300.
17. Gandia C, Arminan A, Garcia-Verdugo JM, et al. Human dental pulp stem cells improve left ventricular function, induce angiogenesis and reduce infarct size in rats with acute myocardial infarction. Stem Cells. 2008; 26: 638-45.
18. Lyakhov I, Zielinski R, Kuban M, et al. HER2- and EGFR-specific affiprobes: novel recombinant optical probes for cell imaging. Chembiochem. 2010; 11(3):345-50.
19. Lu J, Yao YY, Dai QM, et al. Erythropoietin attenuates cardiac dysfunction by increasing myocardial angiogenesis and inhibiting interstitial fibrosis in diabetic rats. Cardiovasc Diabetol. 2012; 11:105.
20. Bekeredjian R, Grayburn PA, Shohet RV. Use of ultrasound contrast agents for gene or drug delivery in cardiovascular medicine. J Am Coll Cardiol. 2005; 45(3): 329-35.
21. Chen S, Shohet RV, Bekeredjian R, et al. Optimization of ultrasound parameters for cardiac gene delivery of adenoviral or plasmid deoxyribonucleic acid by ultrasound-targeted microbubble destruction. J Am Coll Cardiol. 2003; 42(2):301-8.
22. Fujii H, Li SH, Wu J, et al. Repeated and targeted transfer of angiogenic plasmids into the infarcted rat heart via ultrasound targeted microbubble destruction enhances cardiac repair. Eur Heart J. 2011; 32(16): 2075-84.
23. Geis NA, Katus HA, Bekeredjian R. Microbubbles as a vehicle for gene and drug delivery: current clinical implications and future perspectives. Curr Pharm Des. 2012; 18(15): 2166-83.
24. Christiansen JP, French BA, Klibanov AL, et al. Targeted tissue transfection with ultrasound destruction of plasmid-bearing cationic microbubbles. Ultrasound Med Biol. 2003; 29(12): 1759-67.
25. Nomikou N, Tiwari P, Trehan T, et al. McHale. Studies on neutral, cationic and biotinylated cationic microbubbles in enhancing ultrasound-mediated gene delivery in vitro and in vivo. Acta Biomaterialia. 2012; 8(3): 1273-80.
26. Jin Q, Wang Z, Yan F, et al. A novel cationic microbubble coated with stearic acid-modified polyethylenimine to enhance DNA loading and gene delivery by ultrasound. PLoS One. 2013; 8(9): e76544.
27. Tlaxca JL, Anderson CR, Klibanov AL, et al. Analysis of in vitro transfection by sonoporation using cationic and neutral microbubbles. Ultrasound Med Biol. 2010; 36(11): 1907-18.
28. Caracciolo G, Callipo L, De Sanctis SC, et al. Surface adsorption of protein corona controls the cell internalization mechanism of DC-Chol-DOPE/DNA lipoplexes in serum. Biochim Biophys Acta. 2010; 1798(3): 536-43.
29. Panje CM, Wang DS, Pysz MA, et al. Ultrasound-mediated gene delivery with cationic versus neutral microbubbles: effect of DNA and microbubble dose on in vivo transfection efficiency. Theranostics. 2012; 2(11): 1078-91
30. Huber PE, Pfisterer P. In vitro and in vivo transfection of plasmid DNA in the Dunning prostate tumor R3327-AT1 is enhanced by focused ultrasound. Gene Ther. 2000; 7(17):1516-25.
31. Greenleaf WJ, Bolander ME, Sarkar G, et al. Artificial cavitation nuclei significantly enhance acoustically induced cell transfection. Ultrasound Med Biol. 1998; 24: 587-95.
32. Manome Y, Nakamura M, Ohno T, et al. Ultrasound facilitates transduction of naked plasmid DNA into colon carcinoma cells in vitro and in vivo. Hum Gene Ther. 2000; 11: 1521-8.
33. Wang GZ, Liu JH, Lü SZ,et al. Ultrasonic destruction of albumin microbubbles enhances gene transfection and expression in cardiac myocytes. Chin Med J (Engl). 2011; 124(9):1395-400.
34. Zhang L, Sun Z, Ren P, et al. Ultrasound-targeted microbubble destruction (UTMD) assisted delivery of shRNA against PHD2 into H9C2 Cells. PLoS One. 2015; 10(8):e0134629.
35. Taniyama Y, Tachibana K, Hiraoka K, et al. Development of safe and efficient novel nonviral gene transfer using ultrasound: enhancement of transfection efficiency of naked plasmid DNA in skeletal muscle. Gene Ther. 2002; 9(6):372-80.
36. Tsai KC, Liao ZK, Yang SJ, et al. Differences in gene expression between sonoporation in tumor and in muscle. J Gene Med. 2009; 11(10):933-40.
37. Apfel RE, Holland CK. Gauging the likelihood of cavitation from short-pulse, low-duty cycle diagnostic ultrasound. Ultrasound Med Biol. 1991; 17(2):179-85.
38. Kobulnik J, Kuliszewski MA, Stewart DJ, et al. Comparison of gene delivery techniques for therapeutic angiogenesis ultrasound-mediated destruction of carrier microbubbles versus direct intramuscular injection. J Am Coll Cariol. 2009; 54: 1735-42.
39. Shimoda M, Chen S, Noguchi H, Matsumoto S, Grayburn PA. In vivo non-viral gene delivery of human vascular endothelial growth factor improves revascularisation and restoration of euglycaemia after human islet transplantation into mouse liver. Diabetologia. 2010; 53: 1669-79.
40. Price RJ, Skyba DM, Kaul S, et al. Delivery of colloidal particles and red blood cells to tissue through microvessel ruptures created by targeted microbubble destruction with ultrasound. Circulation. 1998; 98(13):1264-7.
41. Song J, Chappell JC, Qi M, et al. Influence of injection site, microvascular pressure and ultrasound variables on microbubble-mediated delivery of microspheres to muscle. J Am Coll Cardiol. 2002; 39(4):726-31.
42. Vancraeynest D, Havaux X, Pouleur AC, et al. Myocardial delivery of colloid nanoparticles using ultrasound-targeted microbubble destruction. Eur Heart J. 2006; 27(2):237-45.
43. Lin CY, Liu TM, Chen CY, et al. Quantitative and qualitative investigation into the impact of focused ultrasound with microbubbles on the triggered release of nanoparticles from vasculature in mouse tumors. J Control Release. 2010; 146(3):291-8.
44. Otani K, Yamahara K, Ohnishi S, et al. Nonviral delivery of siRNA into mesenchymal stem cells by a combination of ultrasound and microbubbles. J Control Release. 2009; 133(2):146-53.
45. Pislaru SV, Pislaru C, Kinnick RR, et al. Optimization of ultrasound-mediated gene transfer: comparison of contrast agents and ultrasound modalities. Eur Heart J. 2003; 24(18):1690-8.
46. Nordlie MA, Wold LE, Simkhovich BZ, et al. Molecular aspects of ischemic heart disease: ischemia/reperfusion-induced genetic changes and potential applications of gene and RNA interference therapy. J Cardiovasc Pharmacol Ther. 2006; 11(1):17-30.
47. Pi Y, Goldenthal MJ, Marín-García J. Mitochondrial involvement in IGF-1 induced protection of cardiomyocytes against hypoxia/reoxygenation injury. Mol Cell Biochem. 2007; 301(1-2):181-9.
48. Ylä-Herttuala S, Alitalo K. Gene transfer as a tool to induce therapeutic vascular growth. Nat Med. 2003; 9(6):694-701.
49. Jewell UR, Kvietikova I, Scheid A, et al. Induction of HIF-1alpha in response to hypoxia is instantaneous. FASEB J. 2001; 15(7):1312-4.
50. Schofield CJ, Ratcliffe PJ. Oxygen sensing by HIF hydroxylases. Nat Rev Mol Cell Biol. 2004; 5: 343-54.
51. Wang WE, Yang D, Li L, et al. Prolyl hydroxylase domain protein 2 silencing enhances the survival and paracrine function of transplanted adipose-derived stem cells in infarcted myocardium. Circ Res. 2013; 113(3): 288-300.
52. Dou MY, Qin FZ, Li B. The effect of HIF on myocardial remodelling and heart failure. Chinese Circulation Journal. 2015; 30(11):1125-7.
53. Robador PA, SanJosé G, Rodríguez C, et al. HIF-1-mediated up-regulation of cardiotrophin-1 is involved in the survival response of cardiomyocytes to hypoxia. Cardiovasc Res. 2011; 92(2):247-55.
54. Cai Z, Manalo DJ, Wei G, et al. Hearts from rodents exposed to intermittent hypoxia or erythropoietin are protected against ischemia-reperfusion injury. Circulation. 2003; 108(1):79-85.